Ocean Engineering 266 (2022) 112800

Contents lists available at ScienceDirect

Ocean Engineering

journal homepage: www.elsevier.com/locate/oceaneng

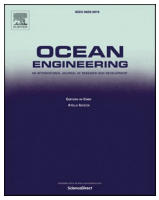

Experimental investigations on the oblique water entry of hollow cylinders

Yu Hou [a], Zhengui Huang [b,*], Zhihua Chen [b], Zeqing Guo [b], Yiming Xu [a]

[a] School of Electrical Engineering, Nantong University, Nantong, 226019, China
[b] National Key Laboratory of Transient Physics, Nanjing University of Science and Technology, Nanjing, 210094, China

ARTICLE INFO

Keywords:
Oblique water entry
Hollow cylinder
Aperture
Cavity evolution
Jet direction

ABSTRACT

The oblique water entry of hollow cylinders with four different apertures is investigated experimentally at low velocities. The evolution characteristics of cavities, jets and splashes with different initial conditions and apertures are disclosed and discussed. The results show that the transition of cavity closure patterns with increasing water-entry velocities is postponed due to the existing water-entry angle. A curved through-hole jet is discovered and its upward ejecting direction can be altered from right to left by different guidance of the inner wall. The cylinder velocities usually increase first, decrease second and recover gradually again. But the final recovery degrees are different with various apertures, water-entry angles and velocities. Under the clockwise moments in the early cavity evolution, hollow cylinders rotate clockwise continuously underwater.

1. Introduction

Some complicated and transient flow phenomena are formed when an object hits and enters the water (Truscott et al., 2014), such as the air-entraining cavity, splash curtain, ejected jets, cavity collapse, etc. They can affect the kinetic stability and deflected trajectory of entry objects in return. Extensive investigations on these water-entry issues have been conducted due to their many practical applications, which exist in daily life, like diving sports (Guillet et al., 2020) and stone skipping (Babbs, 2019; Clanet et al., 2004), in nature, like basilisk lizards water walkers (Glasheen and McMahon, 1996) and plunge-diving seabirds (Louf et al., 2018; Sharker et al., 2019), in industry, like ship slamming (Vincent et al., 2018; Zeraatgar et al., 2019), seaplane landing (Feng et al., 2020), and water-entry aerospace structures (Seddon and Moatamedi, 2006), and in military defense, like aerial torpedoes (Shi et al., 2019; Truscott and Techet, 2009) and anti-submarine projectiles (Guo et al., 2012; Truscott et al., 2009).

The early researches focus on the water entry of typical solid objects based on traditional structures. The solid rigid sphere as a fundamental water-entry model is most studied first. The atmospheric pressure P_0, entry velocity v_0, and sphere diameter D have been deeply studied for the impact force and cavity dynamics in the vertical water entry of spheres (Aristoff et al., 2010; Gilbarg and Anderson, 1948; May and Woodhull, 1948; Truscott et al., 2012). The surface conditions with various contact angles (hydrophilic or hydrophobic) are found significant to determine the cavity formation for water-entry spheres (Aristoff and Bush, 2009; Guleria et al., 2021; Speirs et al., 2019; Zhao et al., 2016). The material (Kim et al., 2020; Yang et al., 2021), the initial rotation (Li et al., 2020; Techet and Truscott, 2011; Truscott and Techet, 2009), the launching mode (Wang and Lyu, 2021; Yun et al., 2020) of spheres can also affect the air-entraining cavity evolution.

With in-depth research, the water entry of other solid objects has also attracted academic and technical researchers' attention widely, such as disks (Bergmann et al., 2009; Gekle et al., 2010), cones (Louf et al., 2018), wedges (Vincent et al., 2018; Zeraatgar et al., 2019), slender cylinders with various nose shapes (Chen et al., 2019; Guo et al., 2012; Yan et al., 2019). Compared to the typical spheres, the geometrical structures, shapes and dimensions of these objects play a leading role in the complicated cavity dynamics and motion kinematics from the past literature review. Recently, a further understanding of geometrical structures' effects on water-entry issues has been extended by the investigations of objects with holes or hollow structures. Some interesting phenomena are found in the water-entry process of these objects, like the trapped air in dimpled spheres (Shokri and Akbarzadeh, 2022), the internal air compressing and expanding in a semi-closed cylinder (Liu et al., 2021; Lu et al., 2016) and through-hole jets in hollow cylinders (Hou et al., 2019, 2021; Jafari and Akbarzadeh, 2022; Zhou et al., 2021). The air-entraining cavity evolution can be more complex and significant with an aperture structure during the water entry.

The water entry of hollow cylinders has been investigated directly since the initial work conducted by Hou et al. (2019). They aim to design a hollow projectile for hitting underwater objects. The hollow projectile

* Corresponding author.
E-mail address: hzgkeylab@njust.edu.cn (Z. Huang).

https://doi.org/10.1016/j.oceaneng.2022.112800
Received 26 July 2022; Received in revised form 25 September 2022; Accepted 2 October 2022
Available online 14 October 2022

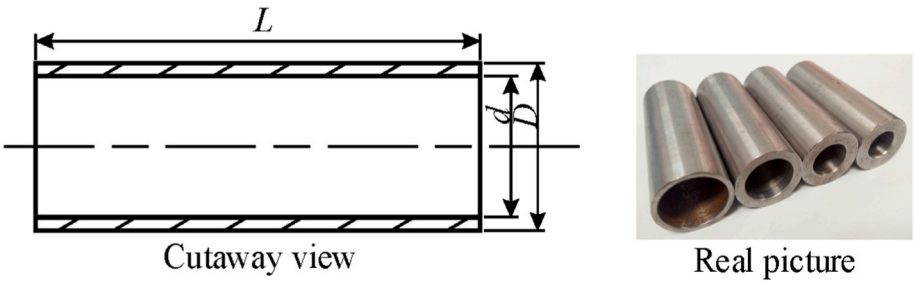

Fig. 1. Schematic of the hollow cylinders.

is a new type of ammunition with a thin-walled circular tube and has more penetration and less fluid drag (Zhao et al., 2019). A lower drag coefficient is discovered numerically in the cavity flow induced by hollow disks with $D_{hole}/D = 0.6$ (Erfanian and Anbarsooz, 2018), which confirms the positive potency of hollow structures in future underwater defense. Hou et al. (2019) find some unique features in the vertical water entry of hollow cylinders, such as a through-hole jet, a trapped bubble on the jet tip and a ringlike tail cavity attached to the geometry. The transition of cavity closure pattern is further analyzed with increasing vertical entry velocities and two types of surface closure are found in Hou et al. (2021). The water-entry issue of hollow objects has attracted more researchers' efforts due to its novelty and fascination. Zhou et al. (2021) investigate the vertical water entry of cylindrical shells with increasing inner diameters numerically and they find that the cavity closure mode changes from the deep-closure to the semi-closed and non-closure mode with various inner diameters. Jafari and Akbarzadeh (2022) investigate the vertical water entry of three hollow projectiles with variable hole shapes experimentally. The highest through-hole jet and the more resistance to cavity sealing are found for the cylinder with a downward conical hole in the same water-entry conditions. These research outcomes can also be indirectly applied in marine and aerospace engineering, such as the water slamming of high-speed crafts with artificial air cavities (Cucinotta et al., 2017) and the recovery of aerospace structures from the sea (Seddon and Moatamedi, 2006).

From the above literature, the previous work focuses on the vertical water entry of hollow cylinders. The air-entraining cavity almost occurs and develops symmetrically with little deflection of the cylinder trajectory and attitude. However, random waves or ripples of the water surface are formed (Feng et al., 2020; Zhang et al., 2020), and the projectile is possible to be disturbed by the propellant impact after the launch. The shooting direction is not always perpendicular to the water surface. Therefore, the projectile is more likely to enter the water at a certain angle actually and the attitude is most inclined to the water surface. The asymmetric force is formed and acts on the entry projectile, which can induce cavity collapse, trajectory instability and attitude rotation (Akbari et al., 2021; Hong et al., 2022; Jiang et al., 2018; Liu et al., 2021; Song et al., 2016, 2020; Truscott et al., 2014). But the influences of the entry angle on the water entry of hollow cylinders have not been well investigated yet. The details of the fundamental flow characteristics and motion kinematics are not clear so far, which is significant for the oblique water entry of hollow projectiles. Therefore, this paper uses the high-speed visualization method to investigate the oblique water entry of the hollow cylinder experimentally. It focuses on the cavity evolution, the jet and splash formation and the cylinder motion characteristics with different cylinder apertures and initial entry velocities.

The paper structure is organized as follows: Section 2 describes the experimental setup, including the test devices, the model dimension and entry conditions. Section 3 mainly shows the results and discussions. Section 3.1 presents the evolution characteristics of oblique water-entry cavities with different closure patterns. Section 3.2 shows the cavity shape variations with different entry velocities and cylinder apertures. Section 3.3 analyzes the formation of curved jets and asymmetric splashes around the water surface. Section 3.4 discusses the inclined motion and the clockwise rotation of hollow cylinders underwater respectively. Finally, Section 4 summarizes the main findings.

Table 1
Details of the hollow cylinders.

Model	D[mm]	D[mm]	d/D	L[mm]	M[kg]
M1	30.0	25.3	0.84	80.0	0.128
M2	30.0	21.3	0.71	80.0	0.220
M3	30.0	17.3	0.58	80.0	0.296
M4	30.0	15.3	0.51	80.0	0.328

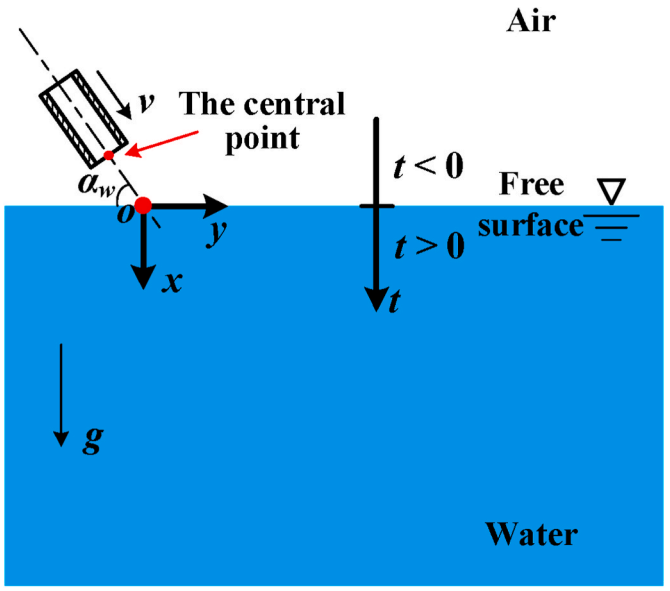

Fig. 2. Schematic of the oblique water entry.

2. Experimental setup

As shown in Fig. 1, four hollow cylinders (M1-M4) with decreasing apertures (d) are designed for the experimental investigation in this paper. They are all made of steel ASTM1045 with the same outer diameter (D) and length (L). The material density is $\rho_s = 7850$ kg/m^3 and their detailed geometric parameters are shown in Table .1.

The hollow cylinder falls into the water at an oblique entry velocity, as shown in Fig. 2. The entry location of the central point on the cylinder head is defined as the origin of the displacement. The positive direction of the x and y coordinates are the same as gravity and horizontal forward direction respectively. The impact moment of the central point on the free surface is set as $t = 0$ and the time (t) increases with the hollow cylinder submergence. The experiments are carried out in a water tank and the hollow cylinder falls freely along the chute into the water. The

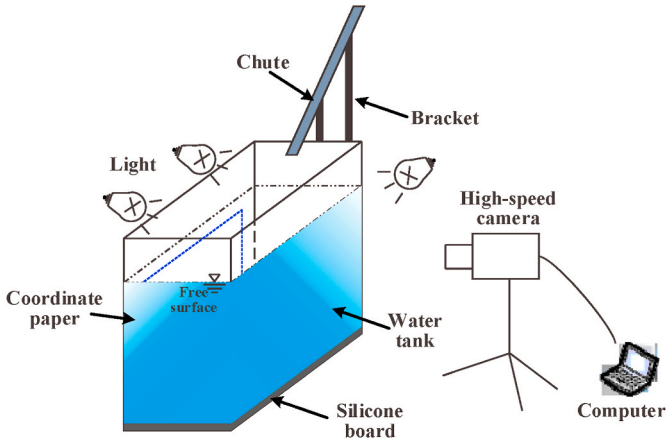

Fig. 3. The experimental system for the oblique water entry of hollow cylinders.

entry velocity is located in the vertical plane (*oxy*) after adjusting the chute direction. The initial velocity is parallel to the center axis of cylinders. The angle between the central axis and the free surface is defined as the water-entry angle α_w.

Details of the experimental system employed are shown in Fig. 3. The whole entry process is captured by a high-speed camera with a frame rate of 2000fps and an image resolution of 1280 × 800 pixels. Enough spotlights are placed around the tank to improve image sharpness under the exposure time of 20 μs. An accurate coordinate paper is used as the reference frame in the photograph background and the image edge detection algorithm based on the Sobel operator is applied to obtain the hollow cylinder location from the photographs. The cylinder displacement can be derived by the pixel coordinate of images based on the calibration values. A quintic spline based on the works of Epps et al. (2010) and Techet and Truscott (2011) is used to fit the captured trajectory data. The velocity ($v(t) = (v_x, v_y)$ m/s) of the cylinders can be obtained from the derivatives of the spline. The experimental tests have been replicated at least three times to ensure the phenomenon reproducibility and measurement accuracy. The average value of measurements is the criterion for drawing graphs and discussion. The square root of error variance between the measured data and the average value (Standard deviation) indicates the amount of uncertainty. The following discussions focus on the characteristics of the water-entry cavity evolution and the hollow cylinder motion with few lateral movements in the *oxy* plane.

In this work, the characteristic length of hollow cylinders is set as $D_c=(D^2\text{-}d^2)^{1/2}$. The Froude number is $Fr = v_0/(g\bullet D_c)^{1/2} = 5.7\text{–}10.6$, where $v_0 = 2.83\text{–}4.25$ m/s is the initial entry velocity of the hollow cylinder and $g = 9.81$ m/s^2 is the gravity acceleration. The straight-line distance between the exit of the chute and the water-entry point is set as a cylinder length (L). The velocity vector ($\boldsymbol{v_0}$) is assumed to be unchanged approximately before the impact due to the immediate water-entry process. The maximum error between the real value and the measurements is estimated to be less than 5% after repeated calibration in consideration of the refraction effects and pixel resolution.

3. Results and discussions

3.1. Characteristics of the cavity closure patterns

As investigated by Hou et al. (2021), three different closure patterns have been found for the vertical water-entry cavity evolution of a hollow cylinder at various entry velocities: deep closure and two types of surface closure. To explore the oblique water-entry cavity evolution, the following discussions are performed in similar closure patterns. The effects of the cylinder apertures on the cavity evolution are further investigated in this work with various water-entry velocities. Both of them are key parameters that affect the characteristics of the cavity closure pattern. Referring to Hou et al. (2019), cavity evolution is also analyzed in four distinct stages generally: the impact stage, the open cavity stage, the cavity closure stage and the free sailing stage with cavities attached.

3.1.1. Deep closure

For the vertical water entry of a hollow cylinder, deep closure occurs at a small entry velocity ($v_0 \leq 2.84$ m/s), as discovered by Hou et al. (2019). However, some evolution characteristics of air-entraining cavities are altered with the entry angle variation in the oblique case. We take the oblique water entry of M1 ($v_0 = 2.93$ m/s, $\alpha_w = 60°$) in deep closure as an example for discussion. As shown in Fig. 4-Fig. 5, the deep closure occurs and the cavity pinches off from left to right between $t =$ 60–70 ms. Two closure points are formed sequentially.

The impact stage occurs around the free surface. It starts from the impact on the water to the full submergence of the cylinder head. The surrounding fluid obtains enough kinetic energy from the cylinder during the impact and is displaced downward and outward. As shown in Fig. 4, for the oblique case, the left cylinder head first touches the water surface due to the inclined attitude at $t = -3$ ms. Then, the touch region between the cylinder head and the water surface moves from left to right along the arc edge with free-fall movements. The entire head submerges fully and ends the impact stage at $t = 5$ ms. Because the cylinder leans to the left, the front fluid is not only displaced upwards and to the right forming the right splash ($t = 5$ ms) but also mainly extruded downward and rightward. The left fluid below the cylinder obtains less kinetic energy and forms a smaller cavity on the left at $t \leq 5$ ms. The left cylinder head remains almost wetted after hitting the water and there are few splashes induced on the left water surface, as shown in Fig. 4 ($t = -3$ ms–5ms). On the contrary, the right fluid is in front of the moving head and can obtain more kinetic energy from the extrusion. It immediately induces the right splash over the water surface when the right head touches the water and begins to form the right open cavity underwater then ($t = 10$ ms).

As outlined by Hou et al. (2019), the vertical water-entry cavity is formed by the surface impact rapidly between the water and the hollow cylinder head. Though the impact process is violent, the entry cavity

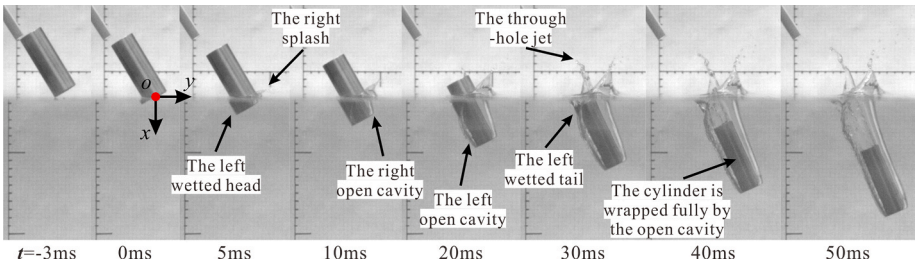

Fig. 4. The deep-closure cavity evolution of hollow cylinders during the oblique water entry (M1, $v_0 = 2.93$ m/s, $\alpha_w = 60°$, $t = -3$-50 ms).

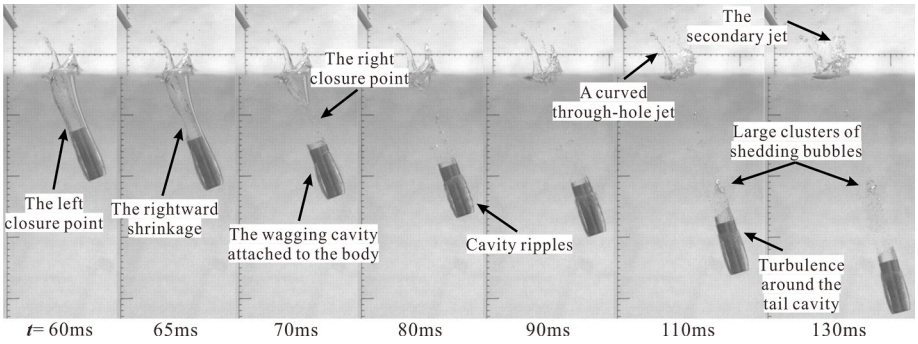

Fig. 5. The deep-closure cavity evolution of hollow cylinders during the oblique water entry (M1, $v_0 = 2.93$ m/s, $\alpha_w = 60°$, $t = 60$–130 ms).

induced is almost symmetrical and evolves axisymmetrically. However, in this oblique case, the initial stage starts from a point impact between the left head and the water. Then, the touch point moves gradually to the other side. During this impact process, the cylinder head plane always intersects the water surface at a certain angle and they collide with each other in a line incessantly. Therefore, the inclined impact process takes more time and acts more gently. It induces the asymmetric hydrodynamic force acting on the hollow projectile and results in different flow characteristics of the oblique entry cavity for both sides of the hollow cylinder.

In the open cavity stage ($t = 5$–50 ms), as shown in Fig. 4, the right fluid gains more kinetic energy than the left during the oblique impact. It forms a right open cavity first underwater at $t = 10$ ms. Then, the open cavity expands towards the left gradually along the outer wall between $t = 10$–30 ms. Its volume increases with the air entrainment. At $t = 20$ ms, the left open cavity occurs and the wetted part of the cylinder fades with the cavity expansion. Only the left cylinder tail is still wetted at $t = 30$ ms due to the backward movements of the cavity boundary point. Finally, the cylinder is wrapped fully by the open cavity at $t = 40$ ms. This stage shows that the oblique open cavity is characterized by the left part forming smaller and occurring much closer to the cylinder than the right. Moreover, the left cylinder head is wetted first in the oblique water entry and enters the cavity after the flow separation. But the right side is always dry and wrapped soon by the open cavity after the impact.

On the other hand, over the water surface, the rising right splashes are induced by the impact at $t = 5$ ms and form a transparent and smooth

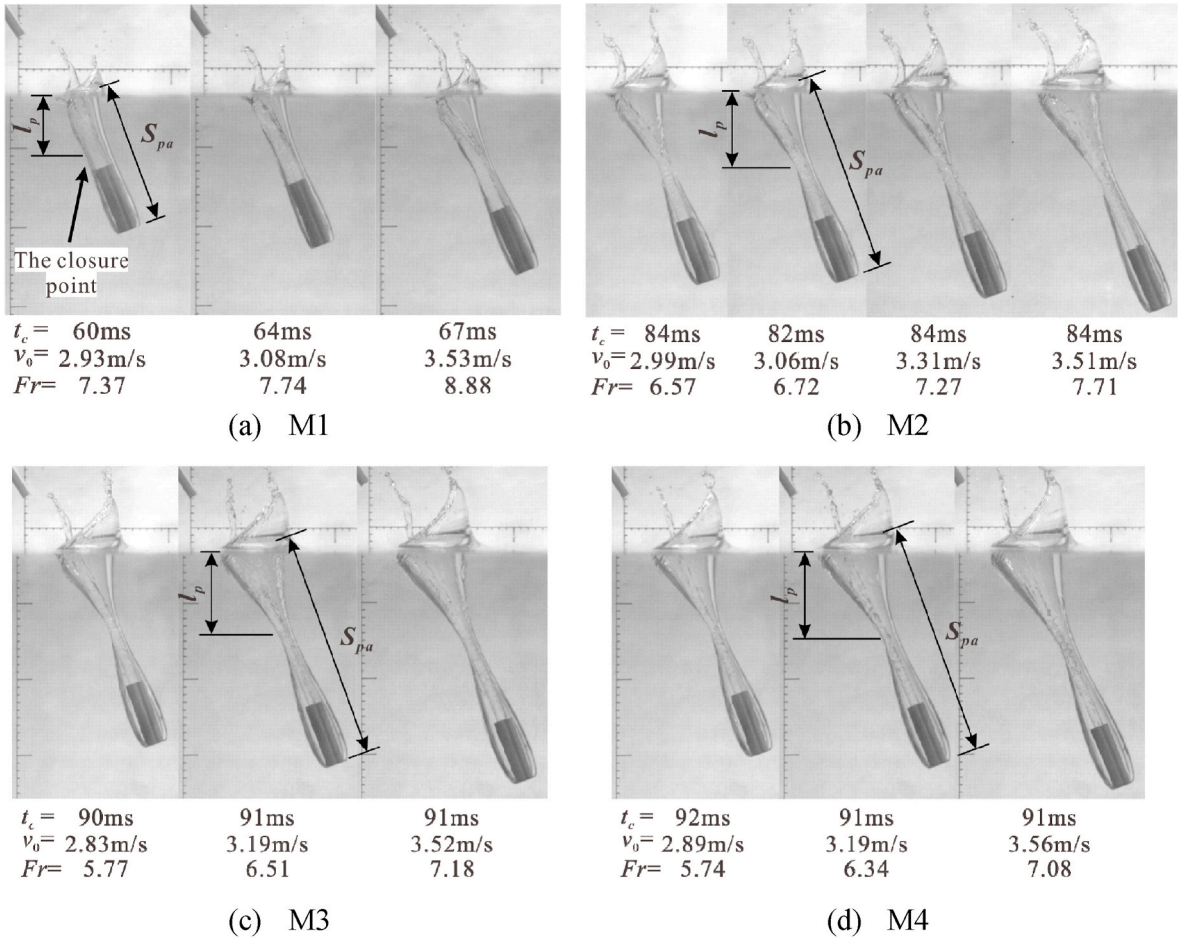

Fig. 6. The cavity comparison of hollow cylinders with decreasing apertures when the deep closure occurs at $\alpha_w = 60°$.

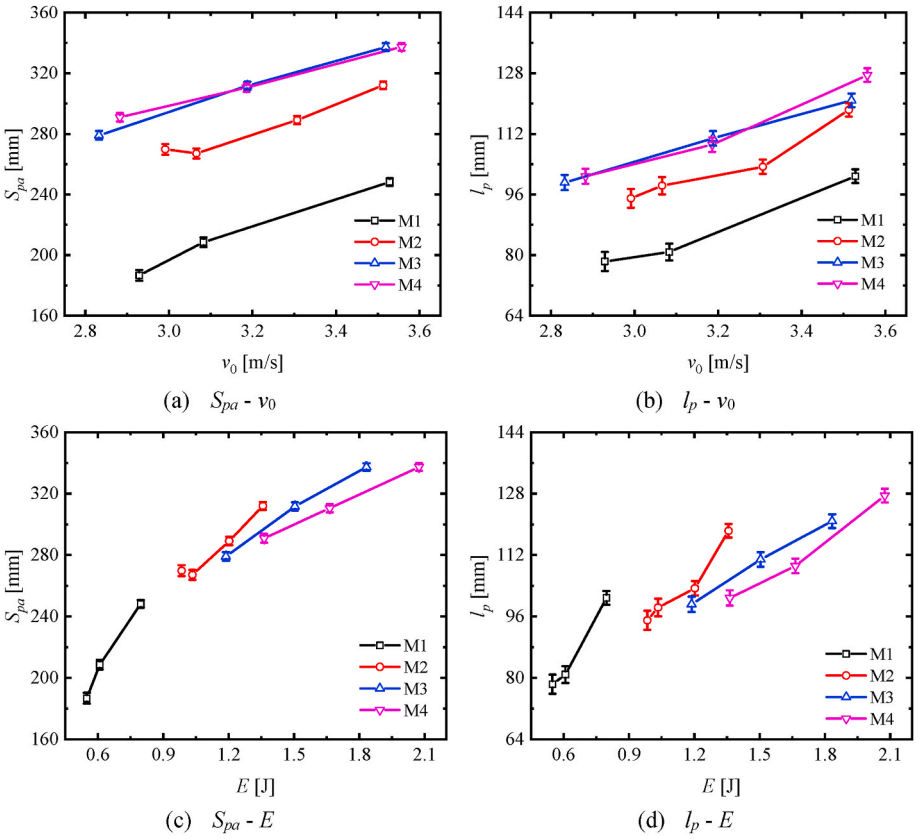

Fig. 7. (a) The submergence distance S_{pa} of cylinders (M1-M4) and (b) the depth l_p of the deep-closure point versus the water-entry velocity v_0 and impact energy E at $\alpha_w = 60°$.

water curtain. The right part is more remarkable and powerful than the left which leads to the splash asymmetry. Its formation mechanism is similar to the open cavity underwater. The flow inside the hollow cylinder induces a through-hole jet along the inner wall at $t = 30$ ms, as shown in Fig. 4. The water-entry process of a hollow cylinder is marked by a distinct jet that passes through the center hole. In this oblique case, the through-hole jet ejects out of the cylinder hole at $t = 20$ ms and has more vertical velocity components than the rising splash. It reaches the same height as the splash tip at about $t = 30$ ms and exceeds after $t = 50$ ms. During the later upward-moving process, the jet column tends to bend left under both gravity and air resistance.

In the cavity closure stage, the cavity expands more weakly and begins contracting after $t = 50$ ms, which results from hydrostatic pressure-driven collapse. As shown in Fig. 5, the left cavity starts to pinch off at $t = 60$ ms before the right. It attributes to two reasons in the previous stages, one is that the left fluid below the inclined cylinder gains less kinetic energy, and the other is that it is mainly displaced to the lower-left region where the hydrostatic pressure is larger than the upper-right. The cavity expansion to the left is weakened more significantly under larger water pressure and the expansion rate decreases faster correspondingly. Thus, the left cavity shrinks and pinches off earlier than the right. Since the left cavity is close to the cylinder wall at the beginning of the closure, it collapses to the geometry tail first and then to the through-hole jet. Then, the cavity contracts rightwards ($t =$ 65 ms) and the closure point moves upward to the right along the jet circumference until $t = 70$ ms. Before the end of pinch-off, the upward and downward parts of the left split cavity have reached the water surface and the cylinder body respectively.

In the free sailing stage with cavities attached ($t > 70$ ms), the inclined cavity contraction induces the asymmetry of left and right cavity length. The contact area between the cylinder sidewall and the water fluctuates alternately. Thus, it generates an asymmetric hydrodynamic force acting on both sides and leads to a cavity waggle. This phenomenon is similar to the cavity swing relative to the body underwater in the tail-slap motion of supercavitating projectiles. However, for this work, the attached cavity waggles more remarkably in the inertial coordinate system. Transient cavity ripples are induced by the rapid cavity contraction at $t = 80$ ms and fade away with the falling cylinder. There are large clusters of bubbles shedding from the attached cavity in the wake flow. The tail cavity is blurred by the laminar-turbulent transition around the interface at $t = 110$ ms, which can also be found in the vertical case (Hou et al., 2019). On the other hand, over the water surface, the upward fluid forms secondary jets on the right of the through-hole jet with the cavity contraction, but still forms no splashes on the left as shown in Fig. 5($t = 130$ ms).

The cavity comparison of hollow cylinders with decreasing apertures is shown in Fig. 6, where $v_0 = 2.8$ m/s~3.6 m/s. The first pinch-off states of the left cavity are captured when the deep closure occurs at $\alpha_w = 60°$.

For all of the cases in Fig. 6, the cavity closure begins with the collision between the left cavity and the through-hole jet. But the sequential pinch-off process from the left to right will fade away with decreasing cylinder apertures. Because the narrower through-hole can slenderize the through-hole jet. Then, the cavity closure pattern modifies from pinching off in a circular line to collapsing to a point approximately. They are still part of the deep-closure pattern in principle when v_0 ranges from 2.8 m/s to 3.6 m/s at $\alpha_w = 60°$. However, referring to M1 cases at $\alpha_w = 90°$ in Hou et al. (2021), the surface closure pattern has appeared when v_0 increases to 2.96 m/s. It indicates that the closure pattern is affected not only by the water-entry velocity but also by the water-entry angle. When the water-entry angle increases, the surface closure is more probable to occur rather than the deep closure at the same water-entry velocity.

On the other hand, when the aperture is large (M1-M3), the deep-closure time increases generally with decreasing apertures. However,

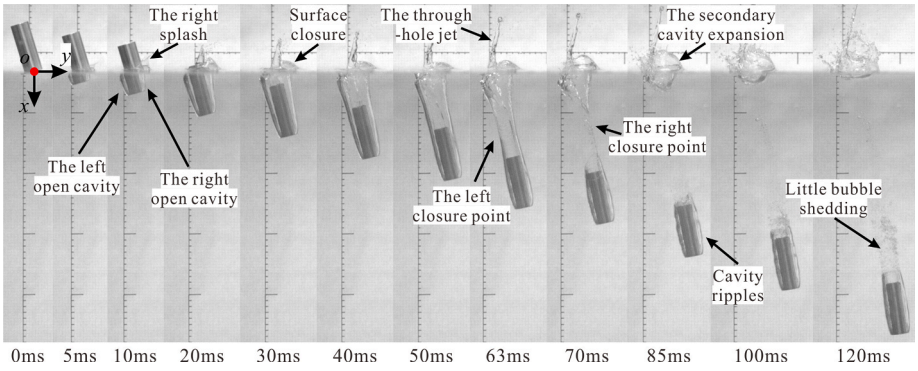

Fig. 8. The surface-closure cavity evolution of hollow cylinders during the oblique water entry at $v_0 = 3.49$ m/s and $\alpha_w = 75°$.

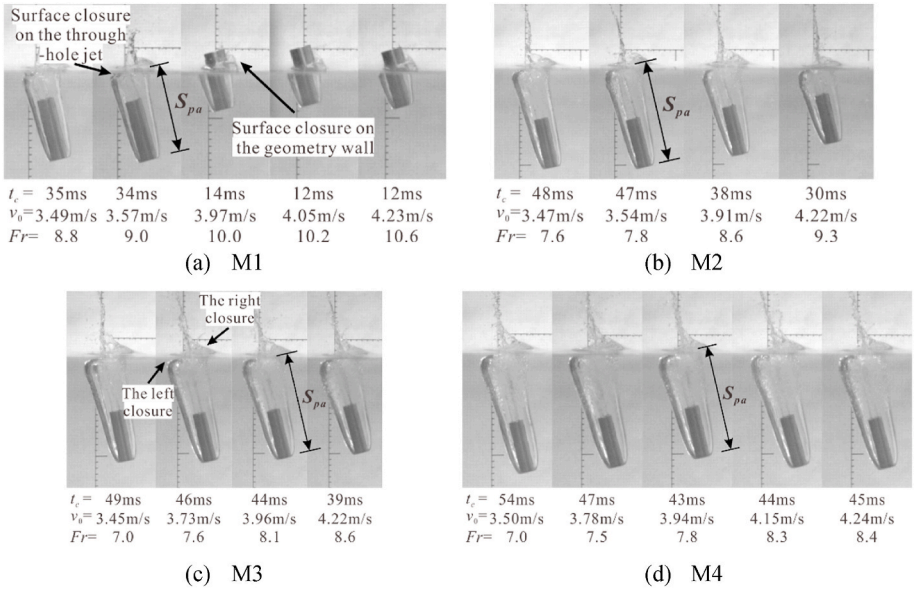

Fig. 9. The cavity comparison of hollow cylinders with decreasing apertures when the surface closure occurs at $\alpha_w = 75°$.

the increasing trend fades away when the aperture is small. For example, the closure time of M3 and M4 is approximately the same and fluctuates around $t = 91$ ms in Fig. 6(c)–(d).

When the deep closure occurs at $\alpha_w = 60°$ (M1-M4), variations of the submergence distance S_{pa} and the closure point depth l_p with the increasing v_0 and impact energy $E = 0.5Mv_0^2$ are shown in Fig. 7. As marked in Fig. 6, S_{pa} is the straight-line distance between the cylinder head center and the water-entry point, and l_p is the vertical distance between the closure point and the water surface. For the variations versus v_0 in Fig. 7(a)–(b), S_{pa} and l_p of M1-M4 all rise generally with the increasing v_0. The levels of S_{pa} and l_p also increase with the decreasing apertures when the aperture is large (M1-M3). However, when the aperture decreases to a certain value (M3-M4), this increasing range is significantly shortened, S_{pa} and l_p levels of M3 and M4 are almost the same. For the variations versus E in Fig. 7(c)–(d), S_{pa} and l_p of M1-M4 also rise generally with the increasing E. But the increasing rate of S_{pa} and l_p versus E is reduced with decreasing apertures.

3.1.2. Surface closure

As indicated by the above analysis, surface closure is more probable to occur when the water-entry angle increases at the same water-entry velocity. Here, we take $\alpha_w = 75°$ as the example for discussion. The oblique water entry of M1 at $\alpha_w = 75°$ is shown in Fig. 8, where $v_0 = 3.49$ m/s and the surface closure on the through-hole jet appears.

The impact stage of this case is similar to the entry process at $\alpha_w = 60°$. It starts from the impact between the left cylinder head and the water surface. Then the intersecting line moves to the right with the falling cylinder until the cylinder head immerges into the water fully. In the open cavity stage, the left cavity is still significantly smaller and closer to the shell wall than the right. However, unlike the sequential cavity formation at $\alpha_w = 60°$, the increasing α_w shortens the immerging time difference between the left and right cylinder head. Thus, the open cavity almost occurs at the same time near both sides. On the other hand, over the water surface, splashes also form only on the right side of the cylinder with a small spray area, as shown in Fig. 8($t = 10$ ms). Their tips converge gradually toward the central axis of the hollow cylinder.

The cavity closure stage starts at $t = 30$ ms. The left displaced fluid and the right spraying splashes both move to the central axis. Then, surface closure on the through-hole jet occurs near the water surface. The closure point on the left side occurs underwater and the right point is on the water due to a certain water-entry angle in the oblique case. It is different from the vertical case with a symmetrical surface closure. A similar deep closure can also be found in the oblique case between $t =$ 63 ms and 70 ms. It induces a secondary cavity expansion near the free surface and forms an attached cavity with little ripples around the cylinder at $t = 85$ ms in Fig. 8. The shedding phenomenon of little bubbles is also captured behind the tail cavity in the following free sailing stage.

The cavity comparison with decreasing cylinder apertures when the surface closure occurs is shown in Fig. 9, where $\alpha_w = 75°$ and $v_0 = 3.45$ m/s~4.25 m/s. Both two types of surface closure are captured in Fig. 9

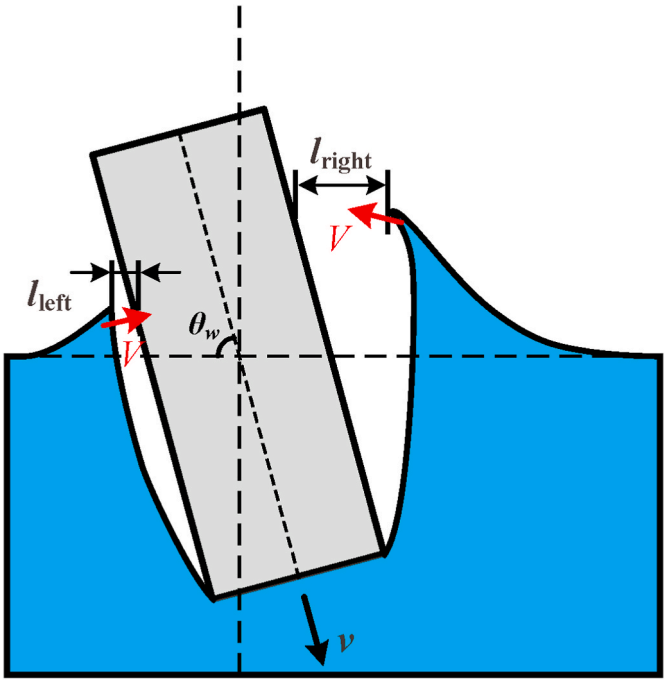

Fig. 10. Schematic of the splash convergence during the oblique water entry.

(a). As performed by the oblique water entry of M1~M4 in Fig. 6, the entry cavity still pinches off in the deep-closure pattern when v_0 increases to about 3.52 m/s at $\alpha_w = 60°$. However, the closure pattern has been modified to the surface closure pattern when v_0 increases to 3.45 m/s at $\alpha_w = 75°$ in Fig. 9. It also confirms that surface closure occurs earlier with the increasing v_0 when α_w is higher.

The increasing v_0 can provide more kinetic energy and accelerate the right splash convergence. When v_0 increases to 3.86 m/s in Fig. 9(a), the surface closure point of M1 has modified from the through-hole jet to the cylinder tail. It changes from surface closure on the through-hole jet to the geometry wall. But the closure pattern of M2-M4 is not modified even though v_0 increases to 4.24 m/s in Fig. 9(c)–(d). It indicates that the decreasing apertures delay the transition of the surface closure pattern with the increasing v_0. The surface closure on the through-hole jet is more probable to appear at a small aperture.

To further illustrate the potential mechanism of this delayed transition, a schematic of the splash convergence during the oblique water entry is shown in Fig. 10. The volume of the right open cavity is visibly larger than that of the left due to a certain water-entry angle. The right distance l_{right} between the splash tip and the cylinder is also longer than the left l_{left}. These characteristics can be seen from the experimental results in Fig. 8. The left splash tip touches the cylinder earlier and more easily obviously than the right during the inward motion towards the cylinder. Thus, whether the surface closure occurs on the geometry wall mainly depends on the right splash tip whether moves fast enough to the cylinder before the full submergence of the cylinder.

From the experimental data, the transient kinetic energy transferred to the fluid particle is increased with decreasing apertures. Then, the cavity near the water surface expands more significantly upward to the right and l_{right} also increases. Therefore, it becomes more difficult for the right splash tip to reach the cylinder in time during the pressure-driven contraction. So it is more difficult for the surface closure on the geometry wall to occur with decreasing apertures actually.

When the surface closure occurs at $\alpha_w = 75°$, variations of the submergence distance S_{pa} of M1-M4 and the surface-closure time t_c with the increasing v_0 and impact energy $E = 0.5Mv_0^2$ are shown in Fig. 11. For the variations versus v_0 in Fig. 11(a)–(b), the value levels of S_{pa} and t_c both rise by leaps with decreasing apertures, but the rising pace slows down

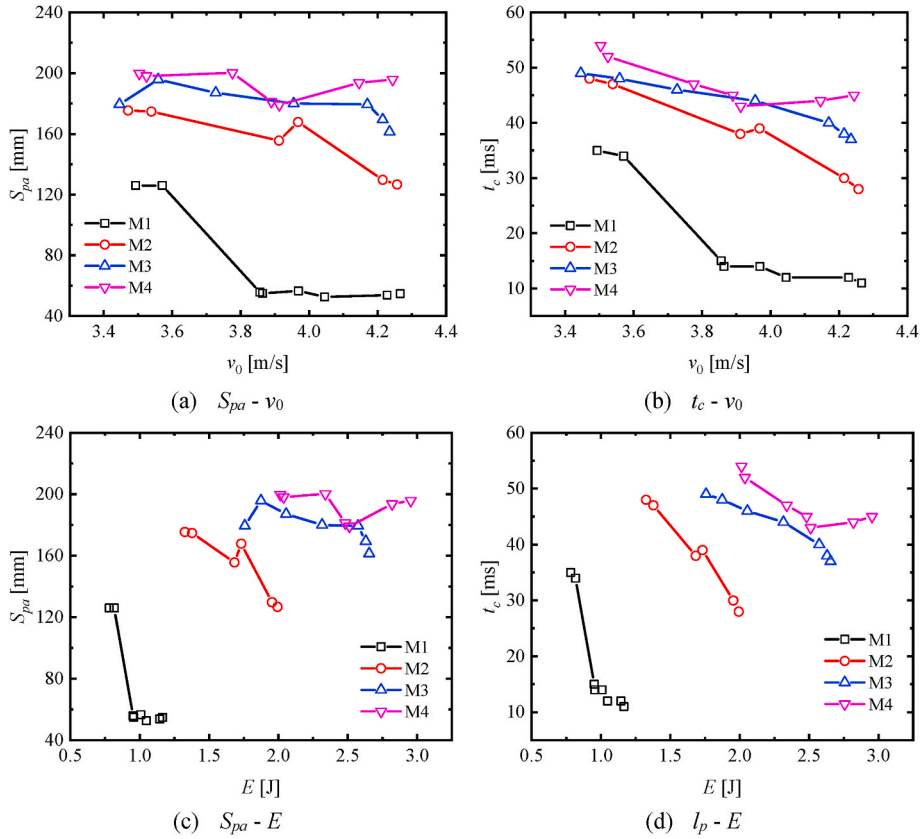

Fig. 11. (a) The submergence distance S_{pa} of cylinders and (b) the surface-closure time t_c versus the water-entry velocity v_0 and impact energy E at $\alpha_w = 75°$.

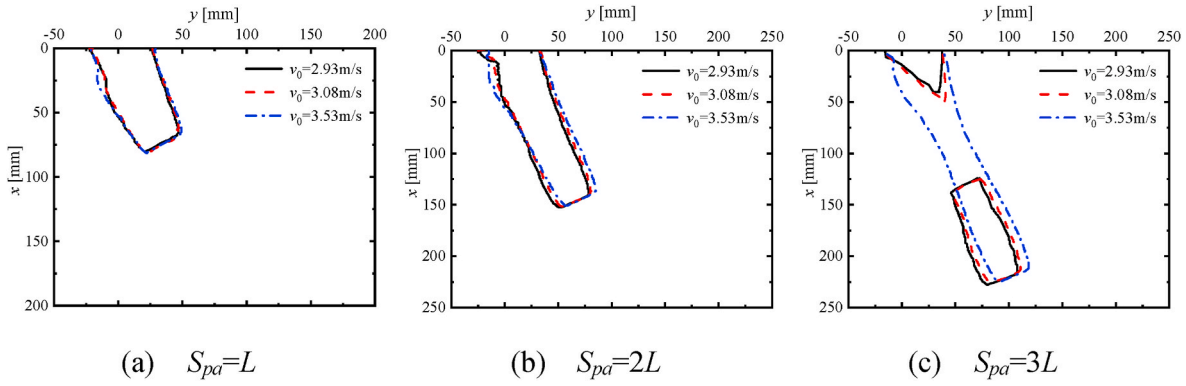

Fig. 12. Variations of the cavity shapes with increasing water-entry velocities ($\alpha_w = 60°$, M1).

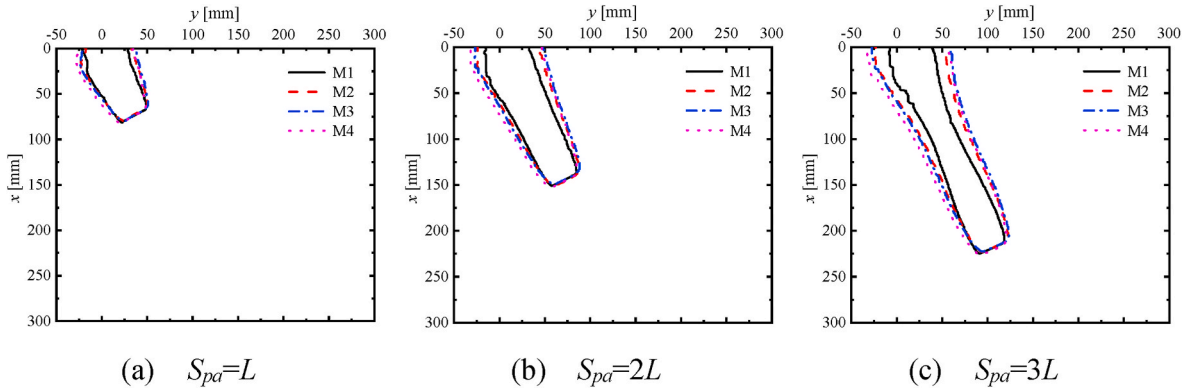

Fig. 13. Variations of the cavity shapes with decreasing cylinder apertures ($\alpha_w = 60°$, $v_0 \approx 3.53$ m/s).

gradually and variations of their values have been close to each other in the water entry of M3 and M4. On the other hand, S_{pa} and t_c both decrease generally with the increasing v_0. However, the decreasing trend fades away when v_0 is high. Such as that S_{pa} and t_c have fluctuated around a certain value at $v_0 > 3.8$ m/s in the water entry of M1. For the variations versus E in Fig. 11(c)–(d), t_c decreases visibly with the increasing E and its decreasing rate is also reduced with decreasing apertures. The decreasing trend of S_{pa} versus E mainly occurs in the water entry of M1 and M2. When the aperture is small (M3 and M4), S_{pa} mainly fluctuates around a certain value versus E.

3.2. The cavity shape variations

The cavity shape variations in the oblique water entry of hollow cylinders at $\alpha_w = 60°$ are shown in Fig. 12 and Fig. 13. The cavity shapes at $S_{pa} = L$, $2L$, and $3L$ are listed in the two figures(a)–(c) respectively. They are mainly captured in the open cavity stage and the cavity closure stage. And the cavities all pinch off in the deep-closure pattern at $\alpha_w = 60°$.

Fig. 12 shows the oblique entry cavity of M1 with increasing water-entry velocities v_0. The outline difference of the head cavity is little with the increasing v_0 at the same S_{pa} in Fig. 12(a). The variations of v_0 mainly affect the closure process and the location offset of the cavity. As shown in Fig. 12(b)(c), the cavity shrinks earlier with the decreasing v_0. The reason is that the decreasing v_0 provides less energy for the fluid particle to move outward and it makes the cavity shrink earlier. On the other hand, the cavity deviates to the lower left more visibly with the decreasing v_0. Because it takes more time for the cylinder with a lower v_0 to reach the same S_{pa}, the cylinder is acted on by gravity and the fluid resistance for a longer time. Its vertical velocity increases and horizontal velocity decreases more distinctly. With a more deflection of the velocity vector, the mass center of the cylinders deviates to the lower left more

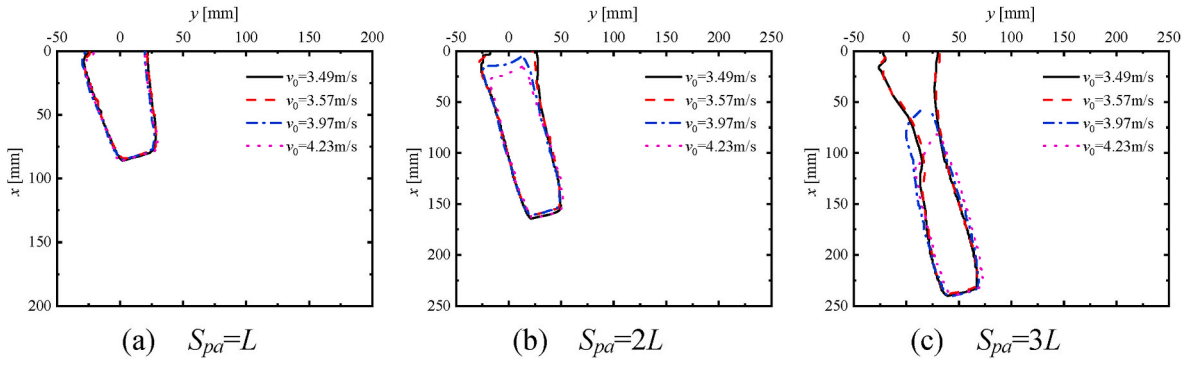

Fig. 14. Variations of the cavity shapes with increasing water-entry velocities ($\alpha_w = 75°$, M1).

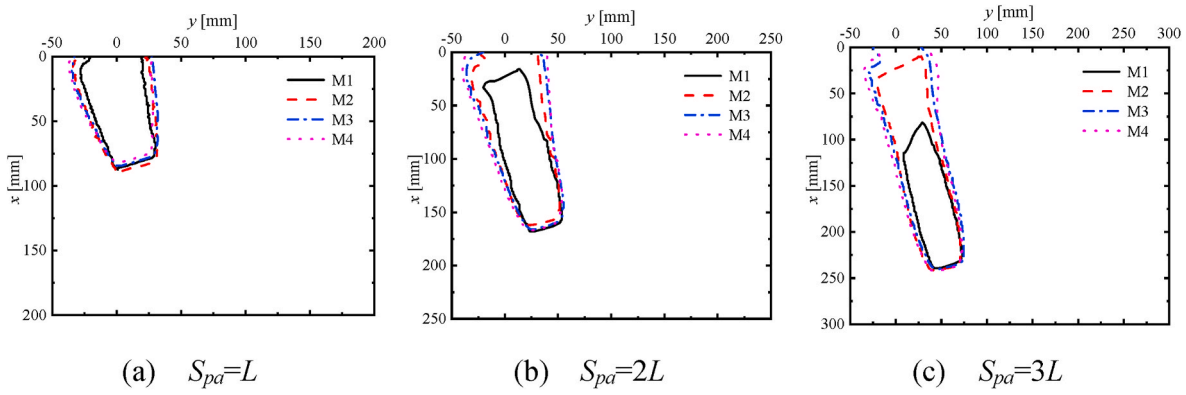

Fig. 15. Variations of the cavity shapes with decreasing cylinder apertures ($\alpha_w = 75°$, $v_0 \approx 4.23$ m/s).

visibly at the same S_{pa}. Correspondingly, the attached cavity deviates to the same location with the decreasing v_0.

Fig. 13 shows the oblique entry cavity of M1-M4 at a similar water-entry velocity $v_0 \approx 3.53$ m/s. As shown in Fig. 13, the decreasing aperture has few effects on the offset location of the cavity and the central axis of the cavities is generally the same in the earlier stage. It mainly alters the cavity diameters and the contraction process. The cavity outlines are wider and the open cavities contract later at the same v_0 and S_{pa} with decreasing apertures. The reason is that the contact area between the cylinder head and the fluid is increased by decreasing apertures. More kinetic energy is transferred to the fluid particles by the transient collision during the water-entry process. The cavity expansion acts more intensely and lasts longer. Thus, the cavity volume is increased and the contraction process is delayed subsequently.

Correspondingly, the experimental data of cavity shape variations at $\alpha_w = 75°$ are also shown in Fig. 14 and Fig. 15. The cavities are all sealed in the surface-closure pattern. Their shapes at $S_{pa} = L$, 2L, and 3L are mainly captured after the surface closure in the two figures(a)–(c) respectively.

Fig. 14 shows the oblique entry cavity of M1 with increasing water-entry velocities v_0. The increasing v_0 has few effects on the outline difference of the head cavity in Fig. 14(a), which is the same as the case at $\alpha_w = 60°$. It also alters the cavity closure process distinctly. When the entry velocities are low ($v_0 = 3.49$ m/s and 3.57 m/s), the cavity outline near $x = 80$ mm expands outwards and then shrinks towards the center axis underwater. When the entry velocities are higher ($v_0 = 3.97$ m/s and 4.23 m/s), the whole cavity has been sealed following the cylinder and contracts gradually with the tail cavity collapse. The cavity outline becomes smaller with the increasing v_0. However, the influences of the v_0 variations on the location offset of the cavity are weakened in the cases. The central axis of cavities and the mass center of cylinders are generally the same except for a few offsets of cavities in Fig. 14(c). It indicates that when α_w is increased from 60° to 75°, the horizontal resistance and displacements of the cylinder are decreased accordingly with the increasing α_w. Fig. 15 shows the oblique entry cavity of M1-M4 with a similar water-entry velocity $v_0 \approx 4.23$ m/s. The cavity shapes are all sealed due to the high entry velocities. The submergence distance S_{pa} of cylinders and the cavity volume are increased with decreasing apertures when the cavity is sealed. The aperture variations also have few effects on the location offset.

In summary, combined with cavity evolutions in the oblique (Figs.12–15) and the vertical (Hou et al., 2021) water entry, the α_w variations mainly affect the location offset of cavities and the offset at the same S_{pa} is more significant with a smaller α_w. The v_0 variations mainly affect the contraction process of the oblique water-entry cavity, and the contraction process occurs earlier with the decreasing v_0. Finally, the aperture variations mainly affect the size of cavity outlines at the same S_{pa}, and the cavity is larger with decreasing apertures.

3.3. Jets and splashes

To further study the characteristics of the jets and splashes formed in the oblique water entry, their transient shapes of M1-M4 at $\alpha_w = 60°$ and 75° are captured with the increasing v_0 in Fig. 16 and Fig. 17. They are

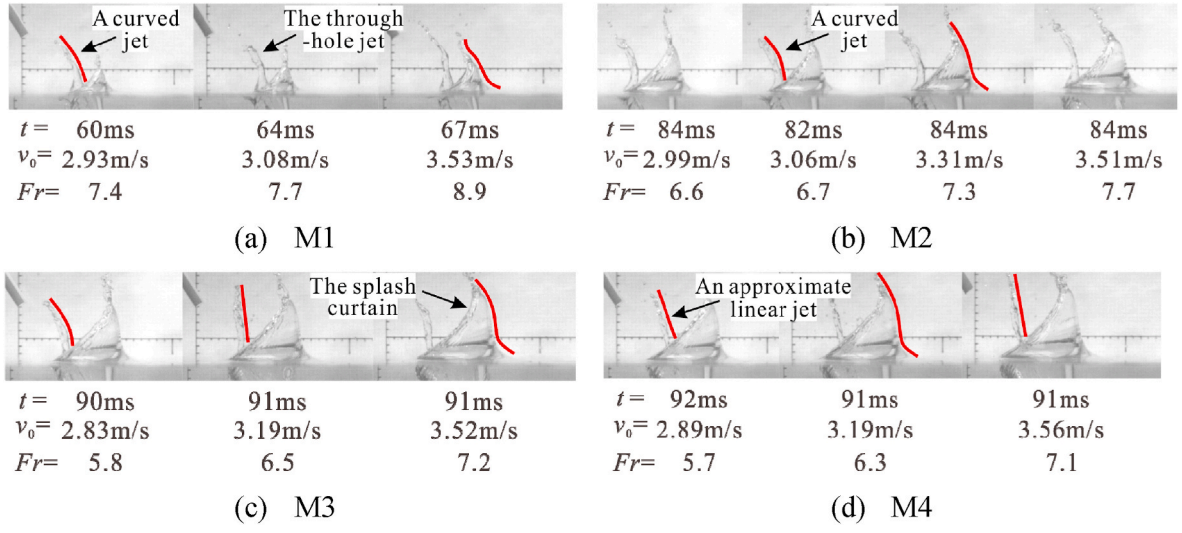

Fig. 16. The jets and splashes induced by the oblique water entry of hollow cylinders at $\alpha_w = 60°$.

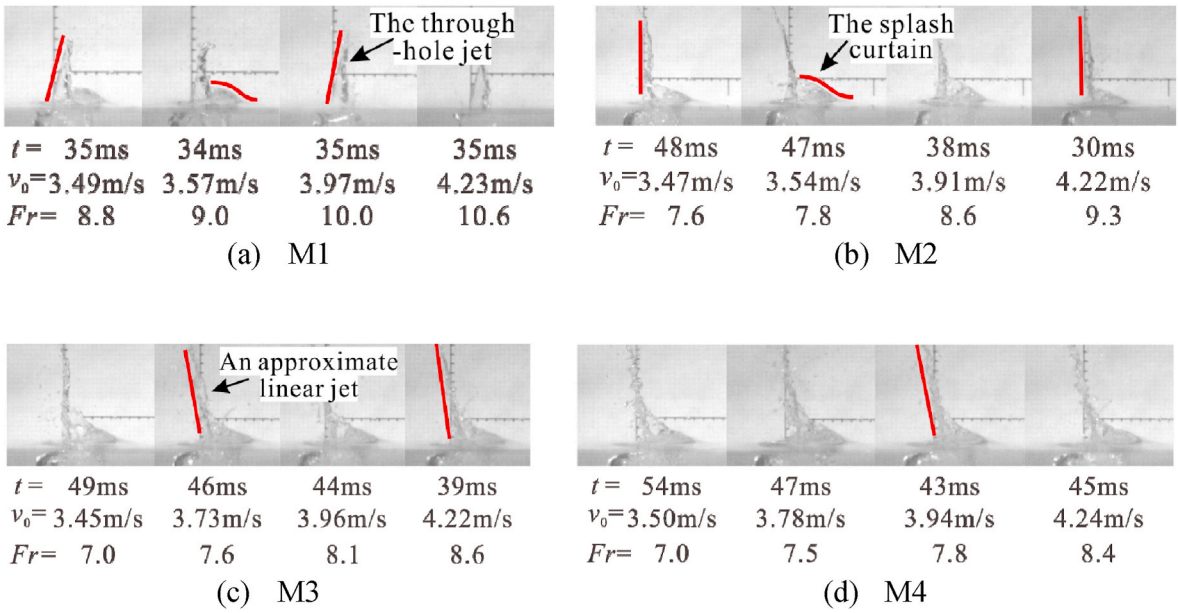

Fig. 17. The jets and splashes induced by the oblique water entry of hollow cylinders at $\alpha_w = 75°$.

both induced by the impact of the cylinder head on the water surface. The jets are formed due to the ejecting fluid through the cylinder hole. The surrounding splashes are mainly formed along the moving direction of the cylinder, that is the area on the right of the through-hole jet in the figures.

Fig. 16 shows the transient shapes of the through-hole jet and splashes in the deep-closure pattern. The through-hole jet ejects out of the water surface in the opposite direction of the water entry. The vertical upward velocity of its top fluid is decreased visibly under gravity and the collision with the inner wall. The jet column is curved gradually from the bottom to the top and the bending offset is more significant with the increasing height in Fig. 16(a)–(c). Moreover, the through-hole jet is slenderized with decreasing apertures and its ejecting direction is more probably affected by the guidance of the inner wall. So that its velocity variations are affected slightly by the inner wall parallel to the ejecting direction approximately. The vertical velocity attenuation of the jet tip also slows down relatively and the bending deformation is postponed accordingly. Thus, the through-hole jet of M4 is approximately linear when the closure occurs in Fig. 16(d).

For the splash evolution, the splash curtain formed near the water surface is just like an inclined transparent funnel when the closure occurs. As shown in Fig. 16, the increasing v_0 and decreasing apertures both result in a higher altitude and a wider range of the splash curtain. The splash tip has tended to converge inward under the pressure difference between the cavity sides.

Fig. 17 mainly shows the transient shapes of splashes and the through-hole jet in the surface-closure pattern. The splash curtain is formed just like a sealed dome with a smaller range near the water surface after the earlier convergence. It is mainly located on the right of the through-hole jet due to the water entry angle. And it sprays lower generally and is relatively closer to the water surface. For the through-hole jets, all of them are mainly formed like a straight line in this case. An interesting phenomenon is further observed: the ejecting direction can be altered remarkably with decreasing apertures. As shown in Fig. 17(a), when the aperture is large (M1), the horizontal velocity of the through-hole jet is consistent with that of the moving hollow cylinder, and the ejecting direction points to the upper right. As shown in Fig. 17(b), when the aperture is decreased, the ejecting direction of M2 rotates anticlockwise gradually and the through-hole jet almost moves vertically upward. After further decreasing the aperture in Fig. 17(c)(d), the ejecting direction continues rotating to the left and is opposite to the entry direction of M3 and M4 approximately. Finally, it becomes the

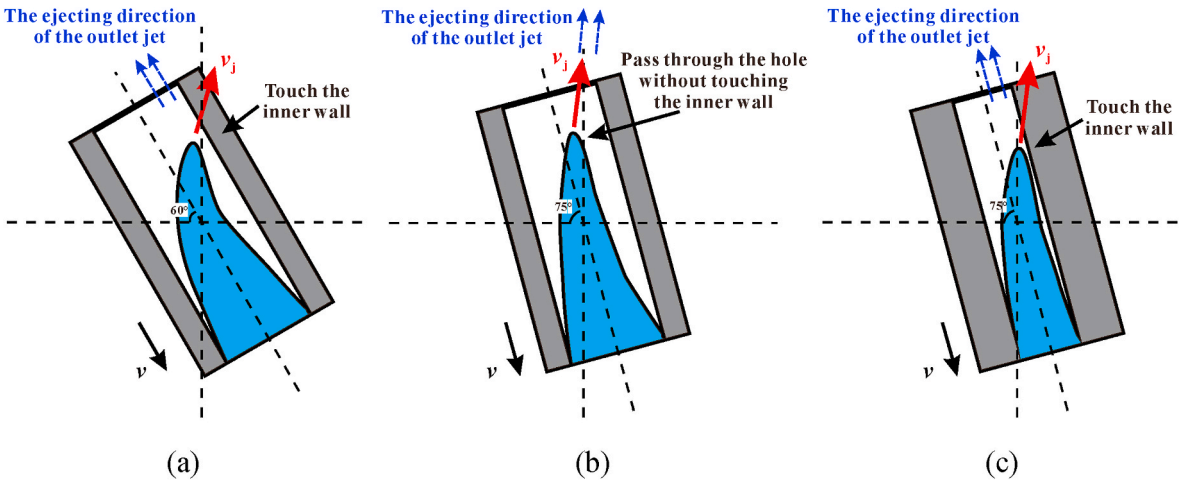

Fig. 18. The ejecting direction of the through-hole jet altered by variations of the water-entry angle α_w and apertures.

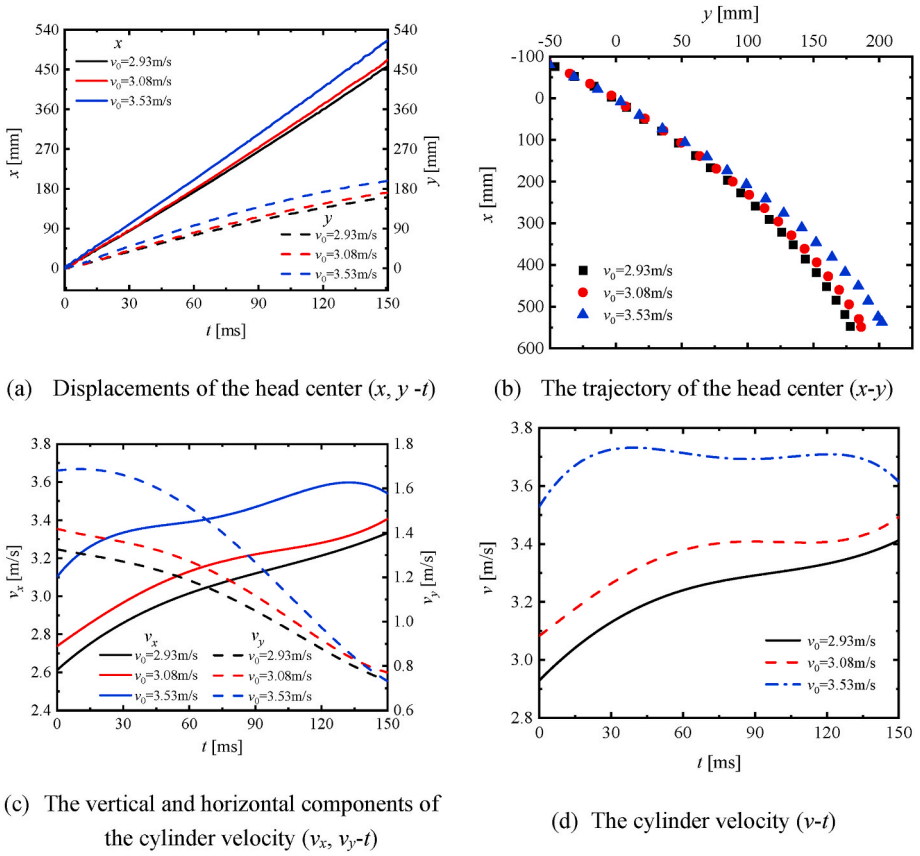

(a) Displacements of the head center (x, y -t)

(b) The trajectory of the head center (x-y)

(c) The vertical and horizontal components of the cylinder velocity (v_x, v_y-t)

(d) The cylinder velocity (v-t)

Fig. 19. Time histories of the moving parameters with increasing water-entry velocities for M1 at $\alpha_w = 60°$.

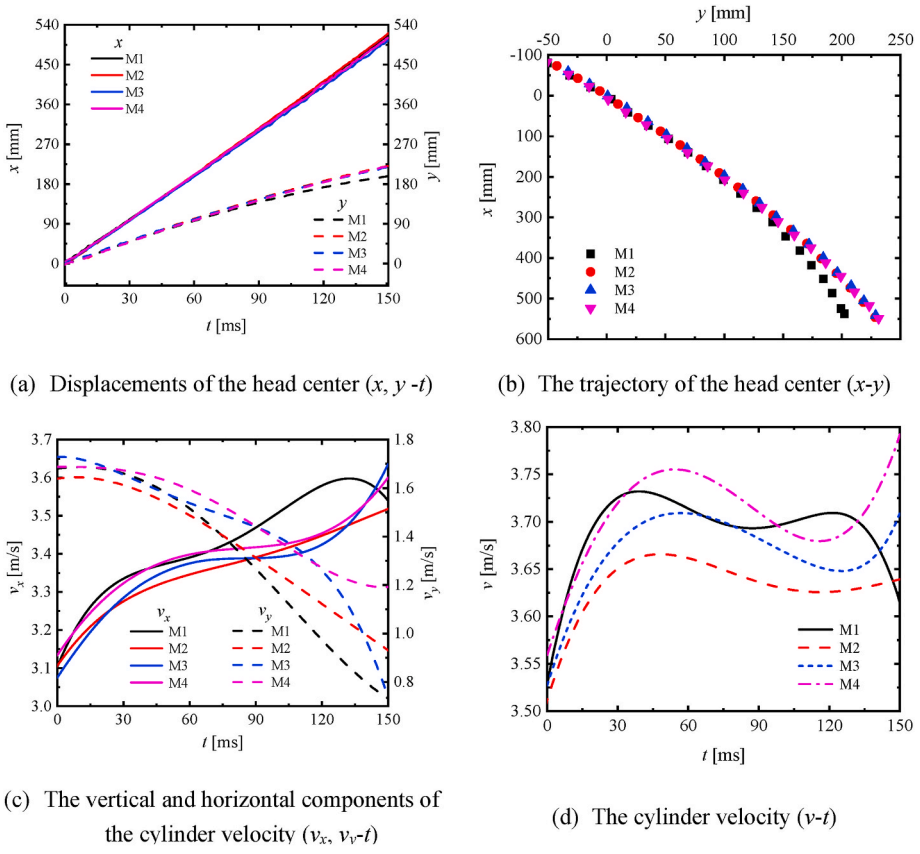

(a) Displacements of the head center (x, y -t)

(b) The trajectory of the head center (x-y)

(c) The vertical and horizontal components of the cylinder velocity (v_x, v_y-t)

(d) The cylinder velocity (v-t)

Fig. 20. Time histories of the moving parameters with decreasing apertures for M1-M4 at $\alpha_w = 60°$ and $v_0 \approx 3.53$ m/s.

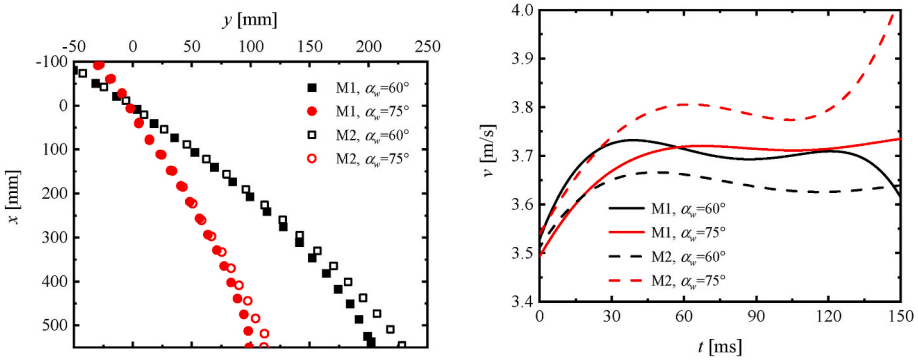

(a) The trajectory of the head center (x-y) (b) The cylinder velocity (v-t)

Fig. 21. Comparisons of moving parameters at $v_0 \approx 3.53$ m/s between $\alpha_w = 60°$ and 75° for M1-M2.

same as the case at $\alpha_w = 60°$ in Fig. 16. However, it seems that the increasing v_0 has few effects on the direction modification in this work.

To further explain the formation mechanism of this interesting phenomenon, a schematic of the ejecting direction altered by variations of the water-entry angle α_w and apertures is shown in Fig. 18. When the cylinder head hits the water, the internal jet tips obtain an initial velocity (v_j) to the left upward generally due to the oblique impact. During the following rising process, when the water-entry angle is lower or the through-hole is more slender, the jets can touch the inner wall more easily before they pass through the hole. As shown in Fig. 18(a) and (c), their ejecting directions (blue arrows) are both altered by the inner wall and opposite to the water-entry direction approximately. However, the jet of the case with $\alpha_w = 75°$ and a larger aperture just can pass through the hole without touching the inner wall in Fig. 18(b). Thus, its ejecting direction remains pointing to the left upward, which is similar to the case in Fig. 17(a). In summary, the ejecting direction of the outlet jet is altered by the guidance of the inner wall on the internal jet.

3.4. The motion characteristics of hollow cylinders

3.4.1. The inclined moving characteristics

To investigate the inclined moving characteristics of hollow cylinders during the water-entry process, variations of the hollow cylinder displacements, trajectories and velocities under different entry conditions are shown in Fig. 19-Fig. 21.

To study variations of the inclined moving parameters with the increasing v_0, we take the oblique water entry of M1 at $\alpha_w = 60°$ as an example for discussion in Fig. 19. As shown in Fig. 19(a), displacements of the head center (x, y) almost increase proportionally versus entry time and their growth rate increases with the increasing v_0. The trajectory of the head center (x-y) is approximately linear before the cylinder enters the water in Fig. 19(b). But it is deflected gradually underwater to the lower left under the horizontal hydraulic resistance. Its deflecting degree becomes higher with the decreasing v_0.

As shown in Fig. 19(c), the cylinder is only under the fluid resistance in the horizontal direction, so the horizontal velocity v_y always decreases versus time. It drops down faster with the increasing v_0 and its values of the three cases have been the same at about $t = 150$ ms. However, not only the fluid resistance but also gravity act on the cylinder in the vertical direction. The vertical velocity v_x increases generally versus time under the dominant gravity. Correspondingly, the vertical displacement (x) of the head center increases faster than y in Fig. 19(a) under gravity. The trajectory (x-y) deflected visibly to the lower left in Fig. 19(b) and it forms an approximate parabolic curve. As the water depth increases, the growth rate of v_x slows down gradually with the rising fluid resistance. In the case at a high water-entry velocity ($v_0 = 3.53$ m/s), since the fluid resistance is significantly larger than that in the other two cases, v_x tends to decrease in the later period. Because v_x is much larger than v_y during the entry motion, the variations of the resultant velocity v are generally similar to that of v_x in Fig. 19(d). The resultant velocity v rises quickly in the early stage and its growth rate gradually slows down later. Due to the larger fluid resistance, v fluctuates visibly in the middle and tends to decrease in the later period in the case at $v_0 = 3.53$ m/s.

To study the variations of the inclined moving parameters with decreasing apertures, we take the oblique water entry of M1-M4 at $\alpha_w = 60°$ and $v_0 \approx 3.53$ m/s as an example for discussions in Fig. 20. As shown in Fig. 20(a) and (b), the decreasing apertures have few effects on the displacements of the head center. Except a few trajectory deviations for M1, the displacements and trajectories of M2-M4 are almost the same. The cylinder velocities (v) all increase visibly under the dominant gravity ($t < 60$ ms) generally in Fig. 20(d). Then, they all decrease gradually under the increasing fluid resistance with the increasing water depth. After the deep closure at $t = 70$–90 ms, the attached cavity is formed and the cylinder velocities(v) increase visibly again under the dominant gravity.

The decreasing apertures mainly affect the later variation of cylinder velocities. Two types of velocity tendency can be found at $t > 120$ ms in Fig. 20(d): increase sequentially or decrease inversely. According to the cavity shapes in Fig. 13, the cavities formed after the oblique water entry become larger with decreasing apertures. Then, the cylinder is wrapped more completely and the hydraulic resistance is decreased significantly. The cylinder also has more inertia with decreasing apertures. Thus, the cylinder velocities rise faster with decreasing apertures in the later period in Fig. 20(d). For the case of M1, not only the attached cavity formed is smaller but also the cylinder inertia is lower. Therefore, the cylinder is decelerated more significantly by the fluid resistance with the increasing water depth. Its velocity (v) decreases shortly after increasing at about $t = 130$ ms and has a distinct decreasing trend in the later period.

To study the influences of the water-entry angle (α_w) on the inclined moving parameters, comparisons of the cylinder trajectories and velocities at $v_0 \approx 3.53$ m/s between $\alpha_w = 60°$ and $\alpha_w = 75°$ for M1 and M2 are shown in Fig. 21. It shows that the cylinder trajectory is deflected to the lower left more remarkably due to the smaller horizontal displacement at $\alpha_w = 75°$ than $\alpha_w = 60°$. For the cylinder velocity, its trend variations are almost the same. The velocities (v) all increase first and decrease shortly generally, and then increase gradually again. Because more horizontal fluid resistance acts on the cylinder in the cases with a lower water-entry angle ($\alpha_w = 60°$), the acceleration effect of gravity is weakened relatively. The velocity growth(v) in these cases slows down relatively at $t > 100$ ms and M1 with lower inertia has tended to decrease actually in the later period.

3.4.2. The rotation characteristics

As performed by the oblique water-entry experiments in Section 3.1, hollow cylinders all rotate clockwise after entering the water. The

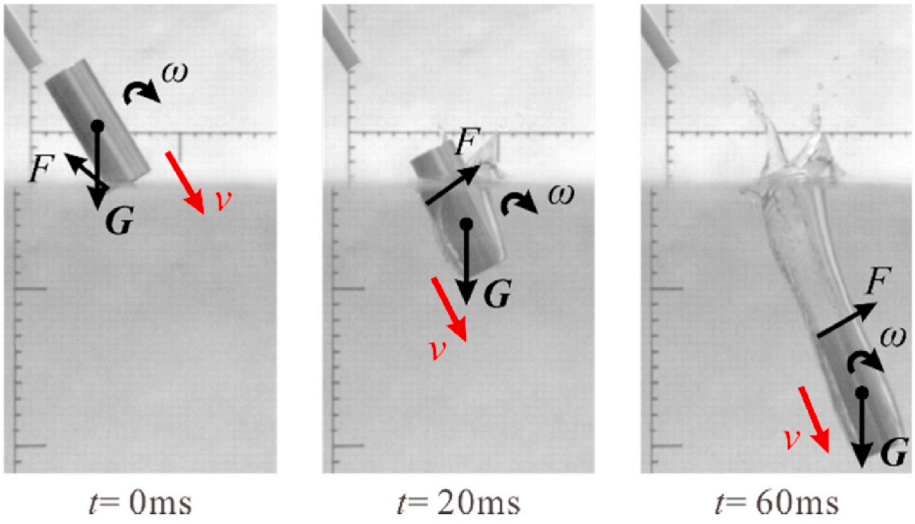

Fig. 22. The cylinder rotation driven by the cavity flow during the oblique water entry.

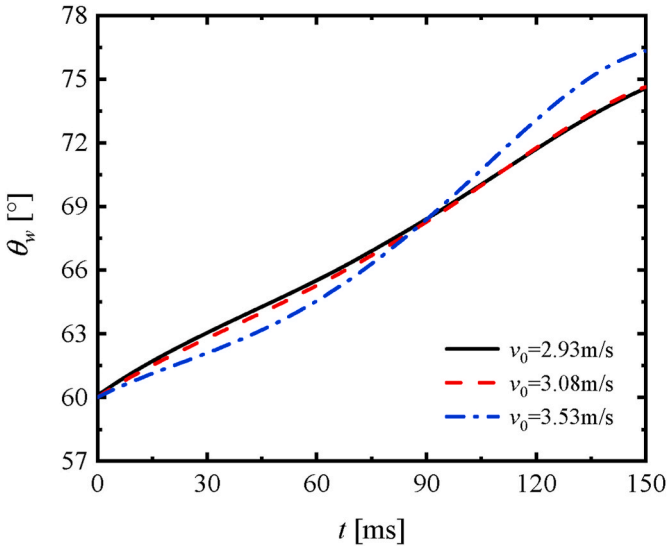

Fig. 23. Variations of the cylinder pitch angle θ_w with increasing water-entry velocities v_0 ($\alpha_w = 60°$, M1).

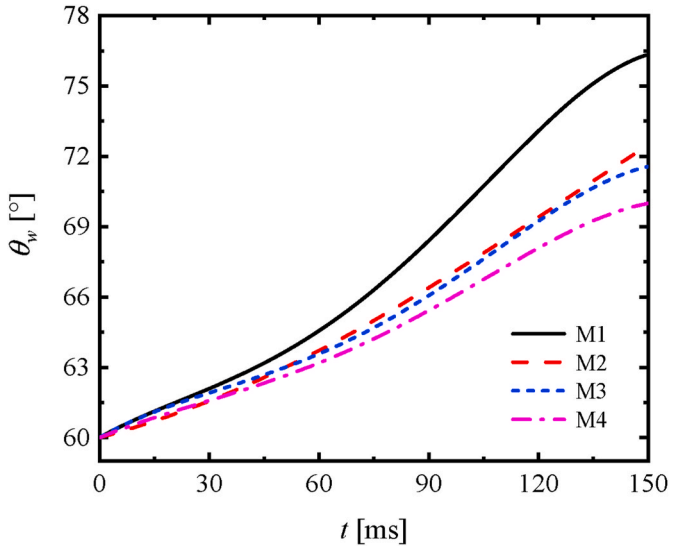

Fig. 24. Variations of the entry pitch angle θ_w with decreasing cylinder apertures ($\alpha_w = 60°$, $v_0 \approx 3.53$ m/s).

interactions between the cylinder and the cavity flow during the oblique water entry are shown in Fig. 22 to illustrate the physical mechanism.

At the initial impact time ($t = 0$ ms), the left head of the cylinders hits the water surface first due to the inclined attitude. The fluid impacts the left head and the left inner wall of the through-hole at the same time. A resultant force pointing to the upper left is formed and acts on the left head. It provides a short clockwise moment relative to the cylinder mass center and then the hollow cylinder rotates clockwise. After the water entry ($t \geq 20$ ms), the contact point between the left cavity and the cylinder wall moves backward gradually with the attached cavity formation. The left rear half of the cylinder remains wet during the moving process. A resultant force pointing to the upper right is formed and acts on the cylinder tail. It provides a lasting clockwise moment for the cylinder again. As shown in Fig. 22, the left cavity pinches off first in the deep-closure case and can impact the left cylinder tail instantly at $t = 60$ ms during the downward contraction. It forms a momentum pointing to the upper right on the cylinder tail and provides an extra transient clockwise moment. Therefore, the hollow cylinder rotates clockwise generally after entering the water obliquely.

Variations of the cylinder pitch angle (θ_w) under different entry conditions are shown in Fig. 23-Fig. 25, where θ_w is the angle between the cylinder center axis and the water surface. It can be calculated from the slope factor of the cylinder head relative to the water surface. Its value is the same as the water-entry angle α_w at the initial impact time. Variations of θ_w present the cylinder rotation around the z coordinate axis in this work. Because hollow cylinders all rotate clockwise after entering the water generally in our cases, the θ_w tends to rise versus time in Figs.23–25.

Fig. 23 shows the θ_w variations of M1 at $\alpha_w = 60°$ with the increasing v_0. The variation curves ($t < 60$ ms) show that the cylinder rotates more slowly in the early stage with the increasing v_0. But after the cavity closure ($t > 60$ ms), the cylinder rotation is accelerated remarkably. The θ_w in the case at $v_0 = 3.53$ m/s catches up with that in other cases soon at about $t = 90$ ms. It indicates that the cylinder rotation driven by the deep closure is accelerated and more significant with the increasing v_0. To study the effects of cylinder apertures on the rotation, the θ_w variations with decreasing apertures (M1-M4) at $\alpha_w = 60°$ and $v_0 \approx 3.53$ m/s is taken as an example for discussion in Fig. 24. The hollow cylinder rotates more difficultly due to the increased rotational inertia with decreasing apertures. Thus, the angular rotation at the same water-entry

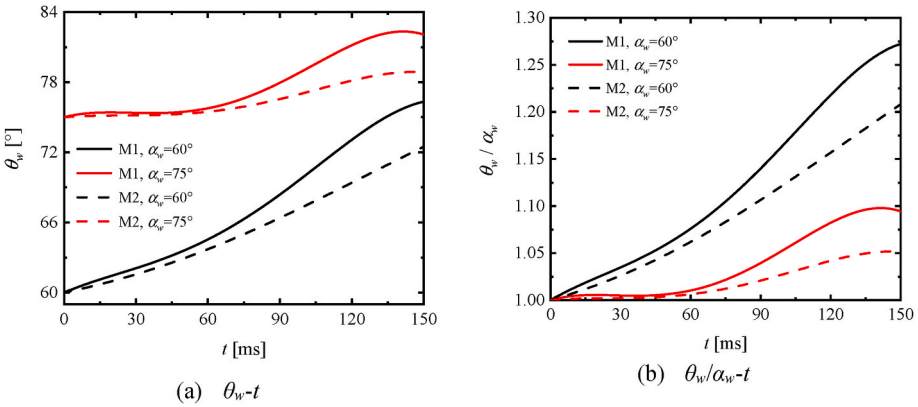

Fig. 25. Comparisons of the entry pitch angle θ_w between $\alpha_w = 60°$ and 75° for M1-M2 at $v_0 \approx 3.53$ m/s.

velocity is decreased visibly with decreasing apertures.

Fig. 25 shows comparisons of the θ_w variations between $\alpha_w = 60°$ and $\alpha_w = 75°$, where Fig. 25(a) shows the real value of θ_w variations and Fig. 25(b) shows the dimensionless value based on the water-entry α_w. We take the water-entry case of M1 and M2 at $v_0 \approx 3.53$ m/s as an example for discussion. It shows that the rotational amplitude of hollow cylinders is increased more remarkably relative to the initial attitude with the decreasing α_w in Fig. 25(b). It indicates that when the water-entry angle is lower, the cylinder attitude recovery towards verticality driven by the hydraulic force is more significant after entering the water.

4. Conclusions

In this paper, the oblique water entry of hollow cylinders with low velocities is investigated experimentally based on high-speed visualization. It shows the effects of the initial water-entry conditions and cylinder apertures on the evolution characteristics of cavities, jets, splashes and the motion characteristics of objects. The transition of cavity closure patterns, the variation of cavity shapes and the alteration of the jet ejecting directions are also disclosed and analyzed. The main findings of this work are summarized as follows:

(1) The cylinder head hits the water gently in a line contact pattern in the oblique impact stage. It induces the asymmetry of the left and right air-entraining cavity on shapes and formation time. The left cylinder wall is wetted visibly in the early water-entry process. The transition of deep closure to surface closure with increasing water-entry velocities is postponed due to the existing water-entry angle. Surface closure is more probable to occur at a high water-entry angle.

(2) The cavity closure time in the oblique water entry is generally increased with decreasing cylinder apertures. But it is approximately the same with decreasing apertures continually. Surface-closure time is shortened more remarkably with increasing water-entry velocities at a large aperture. At the same submergence, the cavity location offset is more visible with a smaller water-entry angle and the cavity sizes become larger with decreasing apertures. The cavity contracts earlier with the decreasing water-entry velocities.

(3) The through-hole jet is curved visibly under gravity in the oblique water entry, but its bending deformation is postponed due to a higher vertical ejecting velocity with decreasing apertures. Its upward ejecting direction can be altered from right to left under different guidance of the inner wall, which is induced by variations of apertures and water-entry angles. The direction tends to be opposite to the water-entry direction approximately at a smaller aperture and water-entry angle. The splashes are mainly formed on the right of jets and their spraying area is larger with the increasing water-entry velocities and decreasing apertures.

(4) Under gravity and hydraulic force, hollow cylinders are generally deflected to the lower left and rotate clockwise continuously after entering the water. The deflecting degree becomes higher with decreasing water-entry velocities. The angular rotation relative to the initial attitude rises with smaller entry angles and increasing apertures. The cylinder velocities usually rise first, fall second and recover gradually again in the early stage. But the smaller entry angles, increasing water-entry velocities and apertures can decrease the later recovery degree, and the velocities even fall finally in some cases.

CRediT authorship contribution statement

Yu Hou: Investigation, Experiment, Visualization, Writing – original draft, Writing – review & editing. **Zhengui Huang:** Methodology, Data curation, Validation, Writing – review & editing, Supervision. **Zhihua Chen:** Conceptualization, Supervision. **Zeqing Guo:** Facility support, Data curation. **Yiming Xu:** Supervision.

Declaration of competing interest

The authors declare that they have no known competing financial interests or personal relationships that could have appeared to influence the work reported in this paper.

Data availability

The authors are unable or have chosen not to specify which data has been used.

Acknowledgments

This work is supported by the National Natural Science Foundation of China (No. 12002165), the Major Basic Research Project of Equipment Development Department, Nature Science Youth Foundation of Jiangsu Province (No. BK20210348), and the National Key Laboratory Foundation of Transient Physics (No. 6142604210603).

References

Akbari, M.A., Mohammadi, J., Fereidooni, J., 2021. Stability of oblique water entry of cylindrical projectiles. J. Appl. Fluid Mech. 14 (1), 301–314.
Aristoff, J.M., Bush, J.W.M., 2009. Water entry of small hydrophobic spheres. J. Fluid Mech. 619, 45–78.
Aristoff, J.M., Truscott, T.T., Techet, A.H., Bush, J.W.M., 2010. The water entry of decelerating spheres. Phys. Fluids 22 (3), 032102.
Babbs, C.F., 2019. Stone skipping Physics. Phys. Tea. 57 (5), 278–281.

Bergmann, R., van der Meer, D., Gekle, S., van der Bos, A., Lohse, D., 2009. Controlled impact of a disk on a water surface: cavity dynamics. J. Fluid Mech. 633, 381–409.
Chen, T., Huang, W., Zhang, W., Qi, Y.F., Guo, Z.T., 2019. Experimental investigation on trajectory stability of high-speed water entry projectiles. Ocean Eng. 175, 16–24.
Clanet, C., Hersen, F., Bocquet, L., 2004. Secrets of successful stone-skipping. Nat 427 (6969), 29-29.
Cucinotta, F., Guglielmino, E., Sfravara, F., 2017. An experimental comparison between different artificial air cavity designs for a planing hull. Ocean Eng. 140, 233–243.
Epps, B.P., Truscott, T.T., Techet, A.H., 2010. Evaluating derivatives of experimental data using smoothing splines. In: Proceedings of Mathematical Methods in Engineering International Symposium. MMEI, Lisbon Portugal.
Erfanian, M.R., Anbarsooz, M., 2018. Numerical investigation of body and hole effects on the cavitating flow behind a disk cavitator at extremely low Cheek for cavitation numbers. Appl. Math. Model. 62, 163–180.
Feng, S., Mingzhen, W., Jiaxu, Z., Qi, H., 2020. Numerical simulation method for wave surface landing of seaplane. IOP Conf. Ser. Mater. Sci. Eng. 751 (1), 012061.
Gekle, S., Peters, I.R., Gordillo, J.M., van der Meer, D., Lohse, D., 2010. Supersonic air flow due to solid-liquid impact. Phys. Rev. Lett. 104 (2), 024501.
Gilbarg, D., Anderson, R.A., 1948. Influence of atmospheric pressure on the phenomena accompanying the entry of spheres into water. J. Appl. Phys. 19 (2), 127–139.
Glasheen, J.W., McMahon, T.A., 1996. A hydrodynamic model of locomotion in the Basilisk Lizard. Nat 380 (6572), 340–342.
Guillet, T., Mouchet, M., Belayachi, J., Fay, S., Colturi, D., Lundstam, P., Hosoi, P., Clanet, C., Cohen, C., 2020. The hydrodynamics of high diving. Proceedings 49 (1), 73.
Guleria, S.D., Dhar, A., Patil, D.V., 2021. Experimental insights on the water entry of hydrophobic sphere. Phys. Fluids 33 (10), 102109.
Guo, Z.T., Zhang, W., Xiao, X.K., Wei, G., Ren, P., 2012. An investigation into horizontal water entry behaviors of projectiles with different nose shapes. Int. J. Impact Eng. 49, 43–60.
Hong, Y., Zhao, Z.X., Gong, Z.X., Liu, H., 2022. Cavity dynamics in the oblique water entry of a cylinder at constant velocity. Phys. Fluids 34 (2), 021703.
Hou, Y., Huang, Z., Chen, Z., Guo, Z., Luo, Y., 2019. Investigations on the vertical water-entry of a hollow cylinder with deep-closure pattern. Ocean Eng. 190, 106426.
Hou, Y., Huang, Z., Chen, Z., Guo, Z., Han, L., 2021. Different closure patterns of the hollow cylinder cavities with various water-entry velocities. Ocean Eng. 221, 108526.
Jafari, M.-A., Akbarzadeh, P., 2022. Experimental analysis of water entry problem considering hollow cylinders: the impact of hole geometry. Ocean Eng. 259, 111906.
Jiang, Y.H., Bai, T., Gao, Y., Guan, L.W., 2018. Water entry of a constraint posture body under different entry angles and ventilation rates. Ocean Eng. 153, 53–59.
Kim, S., Kim, D., Kim, H., 2020. Effect of wettability on the water entry problem of aluminum spheres. J. Mech. Sci. Technol. 34 (3), 1257–1263.
Li, D.Q., Zhao, X., Kong, D.C., Shentu, J.Z., Wang, G.Y., Huang, B., 2020. Numerical investigation of the water entry of a hydrophobic sphere with spin. Int. J. Multiphas. Flow 126, 103234.
Liu, H., Pi, J.T., Zhou, B., Chen, L., Fu, Q., Zhang, G.Y., 2021. Experimental investigation on the multiphase flow characteristics of oblique water entry of semi-closed cylinder. Ocean Eng. 239, 109819.
Louf, J.-F., Chang, B., Eshraghi, J., Mituniewicz, A., Vlachos, P.P., Jung, S., 2018. Cavity ripple dynamics after pinch-off. J. Fluid Mech. 850, 611–623.
Lu, Z.L., Wei, Y.J., Wang, C., Sun, Z., 2016. An experimental study of water-entry cavitating flows of an end-closed cylindrical shell based on the high-speed imaging technology. Acta Phys. Sin. 65 (1), 309–323.
May, A., Woodhull, J.C., 1948. Drag coefficients of steel spheres entering water vertically. J. Appl. Phys. 19 (12), 1109–1121.
Seddon, C.M., Moatamedi, M., 2006. Review of water entry with applications to aerospace structures. Int. J. Impact Eng. 32 (7), 1045–1067.
Sharker, S.I., Holekamp, S., Mansoor, M.M., Fish, F.E., Truscott, T.T., 2019. Water entry impact dynamics of diving birds. Bioinspiration Biomimetics 14 (5), 056013.
Shi, Y., Wang, G., Pan, G., 2019. Experimental study on cavity dynamics of projectile water entry with different physical parameters. Phys. Fluids 31 (6), 067103.
Shokri, H., Akbarzadeh, P., 2022. Experimental investigation of water entry of dimpled spheres. Ocean Eng. 250, 110992.
Song, W., Wang, C., Wei, Y., Xu, H., 2016. Experiment of cavity and trajectory characteristics of oblique water entry of revolution bodies. Beijing Hangkong Hangtian Daxue Xuebao/Journal of Beijing University of Aeronautics and Astronautics 42 (11), 2386–2394.
Song, Z.J., Duan, W.Y., Xu, G.D., Zhao, B.B., 2020. Experimental and numerical study of the water entry of projectiles at high oblique entry speed. Ocean Eng. 211.
Speirs, N.B., Mansoor, M.M., Belden, J., Truscott, T.T., 2019. Water entry of spheres with various contact angles. J. Fluid Mech. 862.
Techet, A.H., Truscott, T.T., 2011. Water entry of spinning hydrophobic and hydrophilic spheres. J. Fluid Struct. 27 (5–6), 716–726.
Truscott, T.T., Gomez, J.T., Beal, D.N., Techet, A.H., 2009. Shallow angle water entry of ballistic projectiles. In: 7th International Symposium on Cavitation, USA. Ann Arbor, Michigan, pp. 1–14.
Truscott, T.T., Techet, A.H., 2009. Water entry of spinning spheres. J. Fluid Mech. 625, 135–165.
Truscott, T.T., Epps, B.P., Techet, A.H., 2012. Unsteady forces on spheres during free-surface water entry. J. Fluid Mech. 704, 173–210.
Truscott, T.T., Epps, B.P., Belden, J., 2014. Water entry of projectiles. Annu. Rev. Fluid Mech. 46 46, 355–378.
Vincent, L., Xiao, T.B., Yohann, D., Jung, S., Kanso, E., 2018. Dynamics of water entry. J. Fluid Mech. 846, 508–535.
Wang, X., Lyu, X.J., 2021. Experimental study on vertical water entry of twin spheres side-by-side. Ocean Eng. 221, 108508.
Yan, G.X., Pan, G., Shi, Y., Wang, G.H., 2019. Experimental study on water entry of cylindrical projectiles with different nose shapes. Mod. Phys. Lett. B 33 (9), 1950107.
Yang, L., Wei, Y.J., Wang, C., Xia, W.X., Li, J.C., Wang, Z.L., Zhang, D.H., 2021. Dynamics of the cavity evolution during vertical water entry of deformable spheres. Phys. Fluids 33 (6), 065106.
Yun, H.L., Lyu, X., Wei, Z.Y., 2020. Experimental study on oblique water entry of two tandem spheres with collision effect. J. Visual 23 (1), 49–59.
Zeraatgar, H., Malekmohammadi, J., Javaherian, M.J., Moradi, H., 2019. Sampling rate effect on wedge pressure record in water entry by experiment. Ocean Eng. 179, 51–58.
Zhang, G.Y., Hou, Z., Sun, T.Z., Wei, H.P., Li, N., Zhou, B., Gao, Y.J., 2020. Numerical simulation of the effect of waves on cavity dynamics for oblique water entry of a cylinder. J. Hydrodyn. 32 (6), 1178–1190.
Zhao, Q., Chen, Z.H., Huang, Z.G., Zhang, H.H., Ma, J., 2019. Optimization of the aerodynamic configuration of a tubular projectile based on blind kriging. Sci. Iran. 26 (1), 311–322.
Zhao, S., Wei, C., Cong, W., 2016. Numerical investigation of water entry of half hydrophilic and half hydrophobic spheres. Math. Probl Eng., 5265818, 2016.
Zhou, B., Liu, H., Wang, Y., Wu, Z., Han, X., Gho, W.M., 2021. Numerical investigation on the cavity dynamics and multiphase flow field evolution for water entry of vertical cylindrical shell. J. Fluid Struct. 103, 103208.